

# Implementation of underexpanded jet problems on multiprocessor computer systems

I.A. Graur<sup>a</sup>, T.G. Elizarova<sup>a</sup>, T.A. Kudryashova<sup>a</sup>, S.V. Polyakov<sup>a</sup>, S. Montero<sup>b</sup>

<sup>a</sup> Institute for Mathematical Modeling, Russian Academy of Science, 125047 Moscow, Russia

<sup>b</sup> Instituto de Estructura de la Materia, CSIC, Serrano 121, 28006 Madrid, Spain

Parallel implementation for an axisymmetric supersonic jet simulation is presented. Numerical interpretation is based on the quasigasdynamic equation system. Parallel code is constructed using a domain decomposition technique. The Message Passing Interface standard have been used for organization of interprocessor data exchange. Calculations have been performed on cluster multiprocessor computer systems with distributed memory. Comparison of the numerical and experimental data based on Raman spectroscopy are fulfilled.

## 1. INTRODUCTION

The paper is devoted to the implementation of the numerical methods for the gasdynamic flows for the cluster multiprocessor computer systems with the Message Passing Interface (MPI) standard for organization of interprocessor data exchange. Underexpanded jet flow problem is used as an example of the technique applied. The calculations consist in solving quasigasdynamic (QGD) equations [1,2,3] under the flow conditions that allow the comparisons with the experimental results [4,5].

In the flow under consideration the pressure and density differ sharply from the nozzle exit section to the external parts on the jet. The geometrical configuration of the jet changes dramatically from several microns near the nozzle to several millimetres at the downstream section. These features and the complex shock configuration in the inner part of the jet require the implementation of fine computational grids, together with a large number of iterative steps for the solution convergence. So, the jet problem is time consuming and requires the implementation of a powerful computer system, namely parallel computer. The numerical method implemented here has inner structural parallelism and the use of parallel computers seems natural. The experience of using parallel transputer systems for implementation of QGD equations can be found in e.g. [6]. The use of modern parallel systems for semiconductor simulations is described in [7].

The calculations were carried out with flow conditions that allow comparison with the experimental results obtained at the Instituto de Estructura de la Materia, CSIC. The experimental part, based on high sensitivity Raman spectroscopy mapping, provides absolute density and rotational temperature maps covering the significant regions of the jet: zone of silence, barrel shock, Mach disk and subsonic region beyond the Mach disk [4,5]. The miniature jet diagnostic facility was used.

The comparison between numerical and experimental results shows the adequacy of the equation system and of the associated numerical procedure for treating the problem under consideration.

## 2. COMPUTATIONAL MODEL

The numerical interpretation is based on the QGD equations, constructed as an extension of the traditional Navier - Stokes (NS) equations. QGD equations reduce to NS ones for vanishing Knudsen numbers. For stationary flows, the dissipative terms in QGD equations are similar to NS ones with the additional contribution of order  $O(Kn^2)$ , where  $Kn$  is the Knudsen number [2,3].

The axisymmetric vector form of QGD equations in  $(r,z)$  co-ordinates reads:

$$\frac{\partial U}{\partial t} + \frac{\partial F}{\partial r} + \frac{F}{r} + \frac{\partial F_1}{\partial r} + \frac{\partial E}{\partial z} = \frac{\partial}{\partial z} \tau \left( \frac{\partial}{\partial z} V + p \frac{\partial Q_{p/\rho}}{\partial z} + \frac{p}{\rho} \frac{\partial Q_p}{\partial z} + \frac{1}{r} \frac{\partial r Q_1}{\partial r} + \frac{\partial Q_2}{\partial r} \right) +$$

$$\frac{1}{r} \frac{\partial}{\partial r} \tau \left( \frac{\partial r W_1}{\partial r} + r \frac{\partial r W_2}{\partial r} + p \frac{\partial Q_{p/\rho}}{\partial r} + r \frac{p}{\rho} \frac{\partial Q_p}{\partial r} + r \frac{\partial r Q_1}{\partial z} \right) + \frac{\partial}{\partial r} \tau \left( \frac{\partial r G}{\partial r} + \frac{\partial Q_2}{\partial z} \right) - \frac{2\tau}{r^2} G,$$

where:

$$U = \begin{pmatrix} \rho \\ \rho u_z \\ \rho u_r \\ E \end{pmatrix}, E = \begin{pmatrix} \rho u_z^2 \\ \rho u_z^2 + p \\ \rho u_r u_z \\ u_z(E + p) \end{pmatrix}, F = \begin{pmatrix} \rho u_r \\ \rho u_r u_z \\ \rho u_r^2 \\ u_r(E + p) \end{pmatrix}, F_1 = \begin{pmatrix} 0 \\ 0 \\ p \\ 0 \end{pmatrix}, G = \begin{pmatrix} 0 \\ 0 \\ p u_r \\ 0 \end{pmatrix},$$

$$V = \begin{pmatrix} \rho u_z^2 + p \\ \rho u_z^3 + 3p u_z \\ \rho u_r u_z^2 + p u_r \\ u_z^2(E + 2.5p) + 0.5p u_r^2 \end{pmatrix}, Q_p = \begin{pmatrix} 0 \\ 0 \\ 0 \end{pmatrix}, Q_{p/\rho} = \begin{pmatrix} 0 \\ 0 \\ \gamma p / (\rho(\gamma - 1) Pr) \end{pmatrix},$$

$$W_1 = \begin{pmatrix} \rho u_r^2 \\ \rho u_r^2 u_z \\ \rho u_r^3 \\ u_r^2(E + 2p) \end{pmatrix}, W_2 = \begin{pmatrix} p \\ p u_z \\ 2p u_r \\ 0.5p(u_r^2 + u_z^2) \end{pmatrix}, Q_1 = \begin{pmatrix} \rho u_r u_z \\ u_r(\rho u_z^2 + p) \\ \rho u_r^2 u_z \\ u_r u_z(E + 2p) \end{pmatrix}, Q_2 = \begin{pmatrix} 0 \\ p u_z \\ 0 \\ 0 \end{pmatrix}.$$

Here  $E = \rho(u_r^2 + u_z^2)/2 + p/(\gamma - 1)$ ,  $p = \rho(R/M)T$ ,  $\tau = \mu/p$ ,  $\mu$ - is the viscosity coefficient,  $Pr$  is the Prandtl number,  $\gamma$  is the specific heat ratio,  $M$  is the molar mass,  $R$  is the universal gas constant. The viscosity coefficient has been treated within the variable hard sphere (VHS) model, which leads to a thermal dependence in the form:

$$\mu = \mu_e \left( \frac{T}{T_e} \right)^\omega, \quad \text{where} \quad \mu_e = \mu_{ref} \left( \frac{T_e}{T_{ref}} \right)^\omega.$$

Table 1  
Nozzle exit quantities

Stagnation temperature $T_0(K)$	295.
Stagnation pressure $p_0(kPa)$	100.
Temperature $T_e(K)$	249.2
Pressure $p_e(Pa)$	$3.824 \times 10^4$
Number density $n_e(m^{-3})$	$1.1114 \times 10^{25}$
Mean free path $\lambda_e(m)$	$11.73 \times 10^{-8}$
Mach number $Ma_e$	1.01
Temperature of residual gas $T_\infty(K)$	200.
Knudsen number $Kn = \lambda_e / (2r_e)$	$3.747 \times 10^{-4}$

The VHS molecular diameter  $d_{ref} = d(T_{ref}) = 4.17 \times 10^{-10} m$ ,  $\omega = 0.74$  and  $\mu_{ref} = \mu(T_{ref}) = 1.656 \times 10^{-5} Nsm^{-2}$  at  $T_{ref} = 273K$  according to [8] have been used here for  $N_2$ . The nozzle exit quantities required for the calculation are reported in Table 1. They have been obtained from the conditions of the experiment by means of the isentropic approximation assuming  $Ma_e = u_e / a_e = 1.01$  at the nozzle exit, where  $\gamma = 1.4$ ,  $r_e = 156.5 \mu m$ ,  $p_0 = 1bar$ ,  $T_0 = 295K$ .

Present computational efficiency was tested with respect to the experimental density and rotational temperature profiles of several shock waves, and corresponding wakes, recently reported [4]. These were generated by expansion of nitrogen through a nozzle of exit diameter  $D = 313 \mu m$ , under nominal stagnation pressure ( $p_0$ ), and temperature ( $T_0$ ). The four shock waves used as a reference, henceforth referred to as A, B, C, D were located at distances to the nozzle  $\tilde{z} = z / D$ , of about 9, 18, 27, 36. The locations were fixed by the ratios of stagnation to residual pressure  $p_0 / p_\infty$ , for  $p_\infty = 4.2, 1, 0.5,$

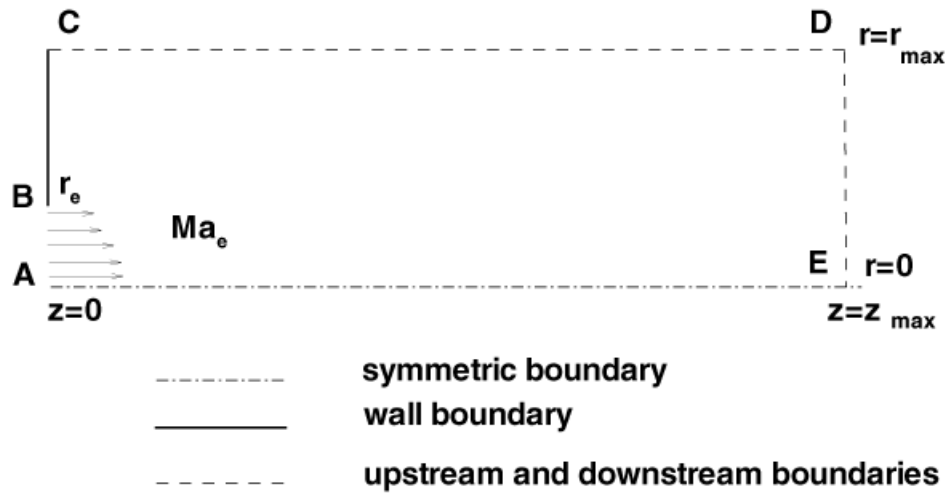


Figure1: Computational domain

0.28 mbar, respectively, controlling the residual pressure by means of an inlet needle valve in the expansion chamber.

The scheme of the computational domain is shown in Figure 1. At the nozzle exit we suppose a laminar boundary layer of width the  $\delta = 0.18r_e$ . The walls of the nozzle are considered to be adiabatic and Crocco's integral has been used for the temperature distribution near the wall [5].

### 3. NUMERICAL ALGORITHM AND PARALLEL REALIZATION

The computational domain is covered with a rectangular grid with space steps  $h_r$  and  $h_z$ . For  $r < r_e$  the grid in the radial direction is uniform, with the smallest space step  $h_r = h_{r,\min} = 0.1r_e$ . For  $r > r_e$ ,  $h_r$  increases between the next cells by a constant factor 1.05. The space step in the axial direction is uniform. The limit of the computational domain in the radial direction is  $r_{\max} = 100r_e$ . The limit of the computational domain in the axial direction corresponds to the experimental conditions. The calculations were carried out for 3 computational grids given in Table 2.

For the solution of QGD equations the upwind – type splitting scheme with the space accuracy  $O(h^2)$  was used based on the dissipative terms of QGD system [9]. The QGD equations are solved by means of an explicit algorithm where the steady-state solution is attained as the limit of a time evolving process. The computations stop when the steady-state solution is achieved.

The high performance parallel computer systems were used here in order to reproduce a detailed flow structure in a reasonable computation time. Present numerical method has been realised as a parallel program. For parallel realisation the geometrical parallelism has been implemented. This means that each processor provides calculations in its own subdomain. The whole computational domain is divided in z-direction. The number of subdomains is equal to the number of processors used.

Suppose that the computer system has  $p$  processors. Grid nodes set in z-direction  $\Omega = \{0,1,\dots,nz\}$  is divided into subsets  $\Omega^{(m)} = \{i_1^{(m)}, \dots, i_2^{(m)}\}$ ,  $m = 0, \dots, p - 1$ . Let  $nr$  is the number of points in r-axis,  $nz$  is the number of points in z-axis. That is, m-processor provides calculations of  $(i_2^{(m)} - i_1^{(m)} + 1) * nr$  points. We form two-dimensional buffers for exchanges of inner boundary data. Data exchange among processors takes place after each time step, providing the synchronisation of the computations. One of the processors collects the results and saves them after each N-time step. If calculations are stopped, they can be continued with the saved files with another processors number (if need). The main sequential program can be included in the developed parallel program. Present software was written in FORTRAN.

Table 2  
Computational grids

Type of grids	1	2	3
Number of points	141*91	281*91	561*91
$h_z / r_e$	1.0	0.5	0.25

All needed parallel functions are contained in MPI parallel libraries.

#### 4. COMPUTATIONAL RESULTS

Two computer systems were used in present computational work:

1) MVS-1000M: 128 processors homogeneous parallel computer system equipped with Alpha-667 microprocessors. The total performance is over 130Gflops. Fast communication links give up to 250MB/sec data transmission rate.

2) Intel Pentium III: 24 processors cluster with distributed memory equipped with Intel Pentium III 600 processors. The total performance is over 14Gflops. Fast communication links give a 12MB/sec data transmission rate.

The speed-up for MVS-1000M and Intel-24 systems is shown in Fig. 2. The real efficiency of parallelisation for explicit schemes is close to 100% for sufficiently great number of computational nodes. Present parallel realisation is relatively simple and can be used for other algorithms based on iterative methods similar to the explicit finite-difference schemes.

According to the experimental data the computations were performed for 4 variants of the residual pressure (A, B, C, D). The grid convergence for variant A is plotted in Figures 3 and 4. The measured and calculated number density along the axis is normalized to the minimal value. For the temperature distributions the measured values are also shown. Note that in the experiment the rotational temperature was measured, but in numerical simulations the averaged temperature was calculated. The mentioned temperatures are close one to another except the vicinity of the shock-wave [5]. Decreasing the space steps leads to the convergence of the numerical results to the experimental values. Temperature is less affected to the grid step variations than the density.

In Figures 5, 6 show the density and temperature distributions for variant B (grid 3). For variants A and B calculated density and temperatures profiles nicely reproduce the

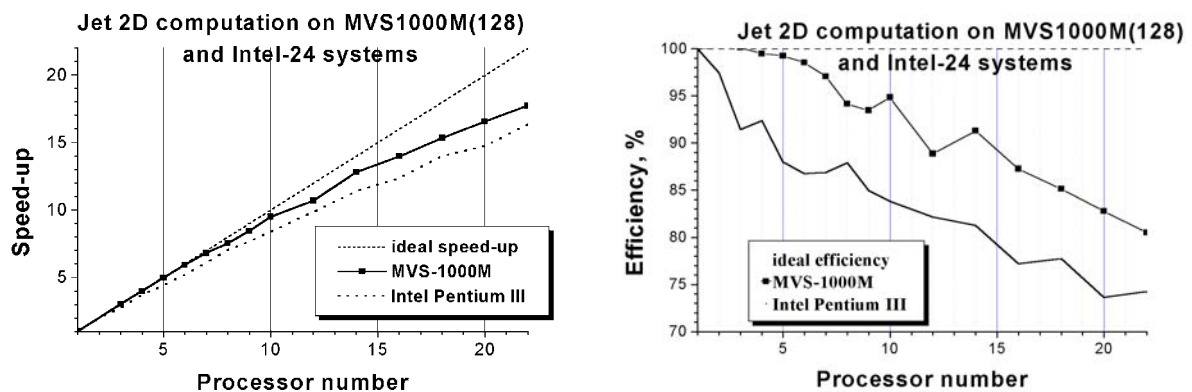


Figure 2: Comparison of parallel performance on MVS-1000M and Intel Pentium III

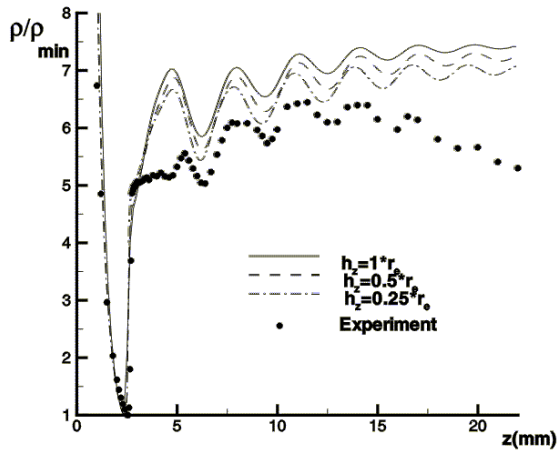


Fig. 3 Density distribution (variant A), grid convergence

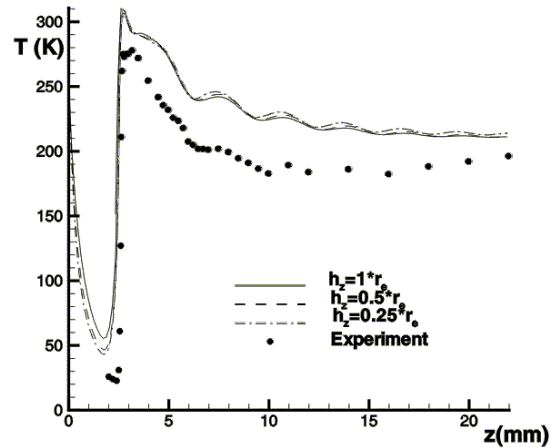


Fig. 4 Temperature distribution (variant A), grid convergence

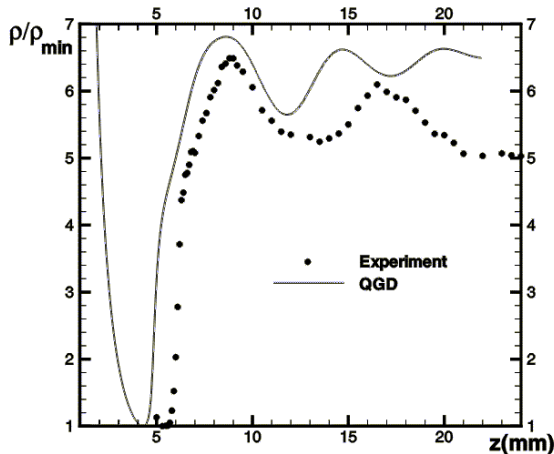


Fig. 5 Density distribution (variant B)

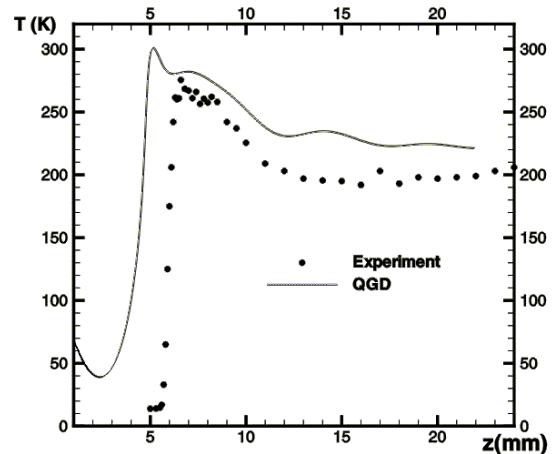


Fig. 6 Temperature distribution (variant B)

experimental data. For variants C and D (not shown here) corresponding to lower residual pressures and larger Kn numbers, the agreement between calculations and the experiment became poorer, especially for the temperature profiles prior to the shock.

Density and velocity maps (variant A, grid 3) presented in Figures 7 and 8, summarise the general features of an axisymmetric supersonic jet, namely zone of silence, Mach disk, barrel shock, slip region behind the Mach disk and the secondary shock waves, that are resolved with a qualitative agreement of the computations with the experiment. A trapped vortex (Fig.8) is formed beyond the Mach disk with a recirculation zone associated with a slow toroidal flow. In this structure the centreline velocity is reversed with respect to that in the zone of silence, differing qualitatively from the post-shock behaviour in one dimension

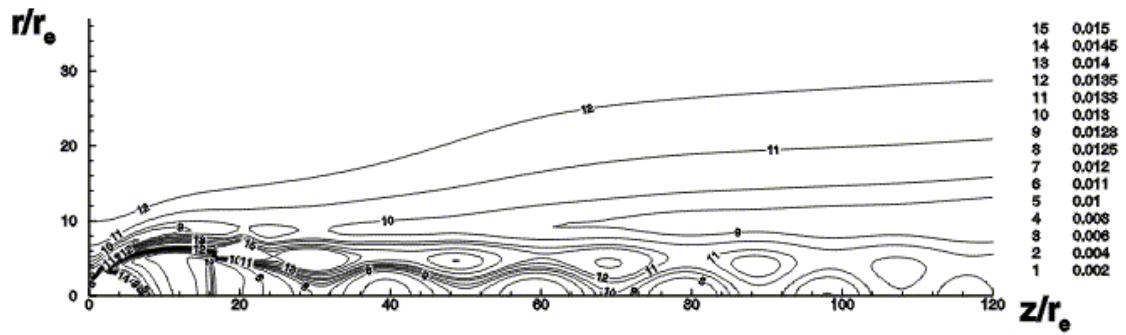


Figure 7: Isolines of density (variant A)

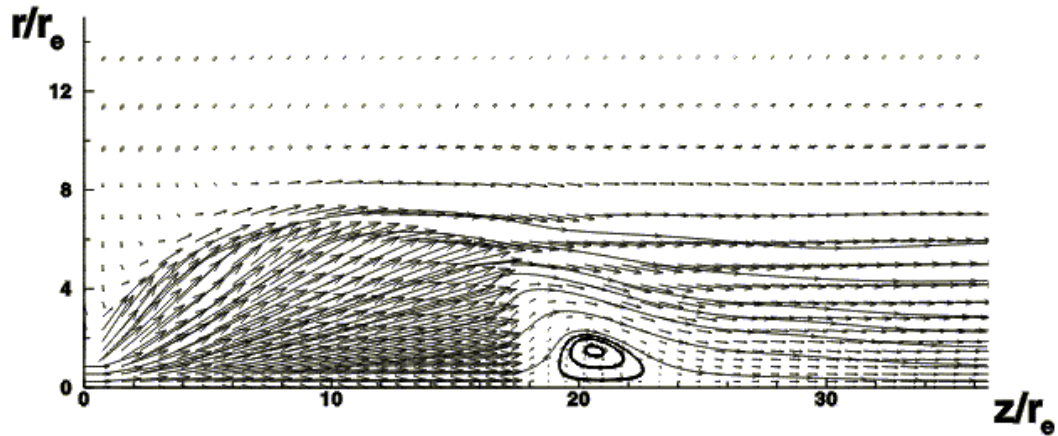


Figure 8: Flow field (variant A)

problem. The toroidal trapped vortex appears to be responsible for the collimation of the jet downstream from the shock wave.

## 5. CONCLUSIONS

The detailed description of an underexpanded jet flow field requires the fine time-space computational grids leading to the time-consuming computations, which naturally demand implementing high-performing computer systems. Present numerical results, and the efficiency estimations, show that the implemented numerical algorithm (explicit in time and homogeneous in space approximation of QGD equations) allows for an efficient use of the cluster multiprocessor computing systems described here.

The comparison of numerical and experimental results shows that the present method is adequate to simulate the underexpanded jet flow for sufficiently small Kn numbers.

## REFERENCES

1. T.G. Elizarova, B.N. Chetverushkin. J. Comput. Math. Phys. Vol. 25, (1985) 164-169.
2. Yu.V Sheretov Quasihydrodynamic equations as a model for viscous compressible heat conductive flows, in book: Implementation of functional analysis in the theory of approaches, Tver University, (1997) 127 - 155 (in Russian).
3. T.G. Elizarova, Yu.V.Sheretov (2001) J. Comput. Math. Phys. Vol. 41, No 2, (2001) 219-234.
4. A. Ramos, B. Mate, G. Tejada, J.M. Fernandez, S. Montero, (2000) Raman Spectroscopy of Hypersonic Shock Waves, Physical Rev E, October, 2000.
5. B. Mate, T.G. Elizarova, I.A. Graur, I. Chirokov, G. Tejada, J.M. Fernandez, S. Montero, J. Fluid Mech., vol. 426, (2001) 177-197.
6. T.G. Elizarova, A.E. Dujsekulov, M. Aspnas, Computing and Control Engineering Journal, 1993, V.4, N 3, pp. 137-144.
7. T.A. Kudryashova, S.V. Polyakov, Simulation of 3D absorption optical bistability problems on multiprocessor computer systems, Proceedings of Moscow State Technological University "STANKIN", General physical and mathematical problems and modeling of technical and technological systems, ed. L.A. Uvarova, Moscow, (2001), 134-146.
8. G.A Bird, (1994), Molecular Gas Dynamics and the Direct Simulation of Gas Flows, Clarendon Press.
9. I.A. Graur (2001), J. Comput. Math. Phys. Vol. 41, No 11 (to be published).